Tikrit Journal of Eng. Sciences /Vol.17/No.3/September2010,(22-30)

Tendons Arrangement Effects on Reinforced Concrete Frames Under Blast Loading

Ayad B. Bahnam
Civil Eng. Dept., College of Engineering, University of Mosul

Abstract

The tendons arrangement effects on the response of reinforced concrete frame experiencing blast loads is investigated in this paper. The structure is modeled using nonlinear finite elements employing a bilinear hysteretic model. So that elements are used so that yielding of the structures could be accurately modeled and captured. The frame is analyzed using a non-linear, elastic-plastic finite element program written in code MATLAB. Six tendon architectures were investigated. A single tendon was placed between different floors and its effects investigated. From the obtained results, the ideal case which causes a reduction in the maximum displacement and the amount of permanent deflection without increase in the maximum structural shear forces greatly is obtained.

Keywords: Tendon arrangement, Reinforced concrete, Blast loading, finite elements.

تأثير ترتيب الأوتار على الهياكل الخرسانية المسلحة تحت تأثير أحمال الانفجار

الخلاصة

يهدف هذا البحث الى دراسة تأثير ترتيب الأوتار على استجابة الهياكل الخرسانية المسلحة المعرضة لأحمال الانفجار. حيث تم دراسة هيكل خرساني مسلح مكون من ثلاثة طوابق وتم نمذجة المنشأ باستخدام العناصر المحددة من خلال استخدام نموذج التخلف ثنائي الخط. إن استخدام مثل هذه العناصر يساعد على نمذجة مرحلة الخضوع للمنشأ بدقة. وتم تحليل المنشأ باستخدام التحليل اللاخطي المرن–اللدن وباستخدام برنامج MATLAB. تم دراسة ست حالات من ترتيب الوتر على منشأ مكون من ثلاثة طوابق، ففي كل حالة تم وضع وتر واحد بين الطوابق لدراسة تأثيره. ومن خلال النتائج التي تم الحصول عليها تم استنتاج الحالة المثالية لترتيب الوتر والتي تؤدي الى تقليل الحد الأعلى من الإزاحات والأود ولا تزيد من قوى القص العظمى في المنشأ بتأثير حمل الانفجار.

Notations

[C] Damping matrix
E Modulus of elasticity
[F] Flexibility matrix
{F} Incremental applied force vector
I Moment of Inertia
[K] Stiffness matrices
$[K_L]$ Linear stiffness matrices
$[K_G]$ Geometric stiffness matrices
[M] Mass matrix
m Mass
[T] Transformation matrix
$\Delta\{\ddot{u}\}$ Incremental acceleration
$\Delta\{\dot{u}\}$ Incremental velocity
$\Delta\{u\}$ Incremental displacement
σ Stress
ε Strain

Introduction

Tikrit Journal of Eng. Sciences /Vol.17/No.3/September2010,(22-30)

In the modern world, the risk of structures experiencing blast loads has increased with a rise in terrorist activities around the world, as well as military actions and the chances of accidental explosions [1]. Numerous blast load hazards present themselves in the form of car bombs, accidental blasting of stored ordnances and numerous other forms of ground shocks [2-4]. As such, it is desirable that modern structures are able to withstand a blast load, particularly relatively distant blasts where the specific structure is not the primary target, but may still suffer extensive damage from the loading.

Blast loads differ from seismic loads in that they excite higher frequency modes, rather than only lower or fundamental frequency modes [5]. As such, damage from blast loads can occur in two stages. First, the initial impact of the blast produces large shear stresses within the structure, which may (if near enough) cause a structure to collapse. Second, after the initial impact of the blast there is a free vibration response, which can produce large non-linear displacements due to the large initial blast induced displacement. Structures can be damaged and/or fail due to excessive non-linear free vibration displacement in this latter stage. Thus, structures that survive the initial blast loading impact can still fail during the free vibration response [2], as both portions of the response are non-linear. Reducing both the initial shear stress and the amount of displacement in the free vibration stage are thus required to best reduce the likelihood of failure.

The response to an impulse load, therefore, has two general phases. The first phase, the forced vibration phase, occurs during the very short application of the impulse. The structure does not reach its maximum displacement in this Phase, as there is not enough time. The second phase, the free vibration phase, occurs after the impulse has been applied. Generally, this phase contains small accelerations and large displacements.

Structural Model

To investigate the effectiveness of tendon arrangement on structures experiencing blast loads, a basic structural analysis computer model was developed as a foundation for these studies. The model accounts for the effects of yielding, plasticity, hysteresis, damping and the excitation of higher frequency local modes. A non-linear finite element model of structure was developed. Due to the nature of blast loads, the modeling technique differs slightly from traditional finite element models of such structures. Blast loads tend to excite the higher frequency modes of the structure on which they act [5]. It is therefore important that the model is able to capture these higher frequencies that are excited by the initial short pulse of the blast load, particularly where they represent local structural modes of columns or beams. This initial pulse also results in initial damage, facilitating failure in the later free vibration response [2].

Giberson One-Component Model

The elements used in the model are based on the Giberson one-component model, as shown in Figure (1) [6]. This model has rigid-plastic rotational springs at each member end. It is assumed that all inelastic deformation occurs at the member ends with the central part of the beam remaining elastic. The incremental flexure rotations at the member ends are obtained from Equation (1), using the Giberson one component model defined in those element equations.

$$\begin{Bmatrix}\Delta\theta_i\\ \Delta\theta_j\end{Bmatrix}_{flexure} = \textit{Elastic flexure rotation}$$

$$+ \textit{Plastic flexure spring rotation}$$

$$= \frac{L}{6EI}\begin{bmatrix}2 & 1\\ 1 & 2\end{bmatrix}\begin{Bmatrix}\Delta M_i\\ \Delta M_j\end{Bmatrix} + \begin{bmatrix}\frac{1}{k_{fi}} & 0\\ 0 & \frac{1}{k_{fj}}\end{bmatrix}\begin{Bmatrix}\Delta M_i\\ \Delta M_j\end{Bmatrix}$$

$$= [f]_{2\times 2}\begin{Bmatrix}\Delta M_i\\ \Delta M_j\end{Bmatrix} \quad \ldots\ldots\ldots (1)$$

Where

$$k_{fi} = \begin{cases}\infty & \textit{Hinge is elastic}\\ 0 & \textit{Hinge is plastic}\\ \frac{EI}{l_p}\left(\frac{r_i}{1-r_i}\right) & \textit{Hinge is inelastic}\end{cases}$$

Where l_p is the plastic hinge length and r_i is the ratio of the inelastic to the elastic stiffness, and all other terms are defined in Figure (2). From Equation (1), the 2 by 2 flexibility matrix, *f*, for each member can be found, the inverse of which will give the stiffness matrix, *K*.

$$[K]_{2\times 2} = [f]^{-1}_{2\times 2} \quad \ldots\ldots\ldots\ldots\ldots (2)$$

The 2 by 2 stiffness matrix becomes a 3 by 3 stiffness matrix when the axial stiffness of the member is considered, denoted by the decoupled *AE/L* term in Equation (3).

$$[K]_{3\times 3} = \begin{bmatrix}\frac{AE}{L} & 0\\ 0 & [K]_{2\times 2}\end{bmatrix} \quad \ldots\ldots\ldots\ldots (3)$$

Rigid End Blocks

When members connect into large structural joints, rigid end block effects should be considered. The assumption of rigid end blocks has a significant effect on the stiffness of a frame, its response to dynamical excitation and its natural frequencies of free vibration. For an elastic member with length L_c the variation of the moment along the rigid end block is assumed to be linear, as given in the following relations.

$$\begin{Bmatrix}u_2^c\\ u_3^c\end{Bmatrix} = \frac{L_c}{6EI}\begin{bmatrix}2 & 1\\ 1 & 2\end{bmatrix}\begin{Bmatrix}S_2^c\\ S_3^c\end{Bmatrix}$$

$$= [f_c]\{S_c\} \quad \ldots\ldots\ldots\ldots\ldots (4)$$

Where:

$[f_c] = \frac{L_c}{6EI}\begin{bmatrix}2 & 1\\ 1 & 2\end{bmatrix}$ Is the flexibility of an elastic member that may be replaced by the flexibility of any inelastic model, such as the Giberson one-component model? The model and parameter definitions with end blocks are shown in Figure (3).

From Figure3, the relationship between the forces at the member end and those of the rigid end blocks can be derived:

$$\frac{x}{x + s_2^c - s_3^c} = \frac{L_1}{L_1 + L_c} \quad \ldots\ldots\ldots (5)$$

$$\frac{y}{y + s_2^c - s_3^c} = \frac{L_2}{L_2 + L_c} \quad \ldots\ldots\ldots (6)$$

Equations (5 & 6) can be rearranged to give:

$$\begin{Bmatrix}s_2\\ s_3\end{Bmatrix} = \begin{Bmatrix}x + s_2^c\\ -y + s_3^c\end{Bmatrix}$$

$$= \begin{bmatrix}1 + \frac{L_1}{L_c} & -\frac{L_1}{L_c}\\ -\frac{L_2}{L_c} & 1 + \frac{L_2}{L_c}\end{bmatrix}\begin{Bmatrix}s_2^c\\ s_3^c\end{Bmatrix}$$

$$= [b]\{s^c\} \quad \ldots\ldots\ldots\ldots (7)$$

Equation (7) can be solved for S^c as:

$$\{s^c\} = [b^{-1}]\{s\} \quad \ldots\ldots\ldots\ldots (8)$$

Now, from the principle of virtual work;

$$\begin{Bmatrix} s_2 \\ s_3 \end{Bmatrix}^T \begin{Bmatrix} u_2 \\ u_3 \end{Bmatrix} = \begin{Bmatrix} s_2^c \\ s_3^c \end{Bmatrix}^T \begin{Bmatrix} u_2^c \\ u_3^c \end{Bmatrix} \quad \ldots\ldots\ldots\ldots (9)$$

Substituting Equation (8) into Equation (9) results in the following expression for the end rotations:

$$\begin{Bmatrix} u_2 \\ u_3 \end{Bmatrix} = \left[b^{-1}\right]^T \begin{Bmatrix} u_2^c \\ u_3^c \end{Bmatrix} \quad \ldots\ldots\ldots\ldots (10)$$

Substituting Equations (4) and (8) into Equation (10) the yields:

$$\begin{Bmatrix} u_2 \\ u_3 \end{Bmatrix} = \left[b^{-1}\right]^T \left[f_c\right] \left[b^{-1}\right] \begin{Bmatrix} s_2 \\ s_3 \end{Bmatrix} = [f]\{s\}. \quad (11)$$

Where [*f*] is the flexibility of the rigid end-blocks, and thus, the stiffness of the member with rigid end-blocks can be determined by inverting the flexibility matrix [*f*].

Coordinate Transformations

Once the flexibility matrix is inverted to find the member stiffness matrix, $[K]_{3x3}$, the stiffness matrix can be transformed using the transformation matrix, [*a*], into the stiffness matrix $[K]_{6x6}$ in the local coordinate system as shown in Figure (4). Then, using the transformation matrix [*T*] the stiffness matrix can be transformed from local coordinates to global coordinates.

$$\begin{Bmatrix} u_1 \\ u_2 \\ u_3 \end{Bmatrix} = \begin{bmatrix} -1 & 0 & 0 & 1 & 0 & 0 \\ 0 & \frac{-1}{L} & -1 & 0 & \frac{1}{L} & 0 \\ 0 & \frac{1}{L} & 0 & 0 & \frac{-1}{L} & 1 \end{bmatrix} \begin{Bmatrix} u'_1 \\ u'_2 \\ u'_3 \\ u'_4 \\ u'_5 \\ u'_6 \end{Bmatrix}$$

……. (12)

Note that the transformation matrix [*a*] is a function of the member length only, shown in Equation (13).

$$a = \begin{bmatrix} -1 & 0 & 0 & 1 & 0 & 0 \\ 0 & \frac{-1}{L} & -1 & 0 & \frac{1}{L} & 0 \\ 0 & \frac{1}{L} & 0 & 0 & \frac{-1}{L} & 1 \end{bmatrix} \ldots. (13)$$

The local coordinates of the member may differ from those of the global system. This point is illustrated in Figure (5) with an angle θ between the two systems.

$$\begin{Bmatrix} u'_1 \\ u'_2 \\ u'_3 \\ u'_4 \\ u'_5 \\ u'_6 \end{Bmatrix} = \begin{bmatrix} \cos\theta & \sin\theta & 0 & 0 & 0 & 0 \\ -\sin\theta & \cos\theta & 0 & 0 & 0 & 0 \\ 0 & 0 & 1 & 0 & 0 & 0 \\ 0 & 0 & 0 & \cos\theta & \sin\theta & 0 \\ 0 & 0 & 0 & -\sin\theta & \cos\theta & 0 \\ 0 & 0 & 0 & 0 & 0 & 1 \end{bmatrix} \begin{Bmatrix} \bar{u}_1 \\ \bar{u}_2 \\ \bar{u}_3 \\ \bar{u}_4 \\ \bar{u}_5 \\ \bar{u}_6 \end{Bmatrix}$$

…….. (14)

This generic transformation matrix [T] is a function of the angle θ only, as shown in Equation (15).

$$[T] = \begin{bmatrix} \cos\theta & \sin\theta & 0 & 0 & 0 & 0 \\ -\sin\theta & \cos\theta & 0 & 0 & 0 & 0 \\ 0 & 0 & 1 & 0 & 0 & 0 \\ 0 & 0 & 0 & \cos\theta & \sin\theta & 0 \\ 0 & 0 & 0 & -\sin\theta & \cos\theta & 0 \\ 0 & 0 & 0 & 0 & 0 & 1 \end{bmatrix}$$

……. (15)

Both transformation matrices, [*T*] and [*a*], are used to convert element matrices into a full system model coordinate system for assembly.

Lumped Mass Model

The four conditions that a mass matrix must satisfy are matrix symmetry, physical symmetries, conservation and positivity. Matrix symmetry means $(M^e)^T = M^e$ for each element. Physical symmetry means the element symmetries must be reflected in the assembled global mass matrix. Conservation means that the total element mass must be preserved

Tikrit Journal of Eng. Sciences /Vol.17/No.3/September2010,(22-30)

in the system model. Higher order conditions, such as conservation of angular momentum, are not critical nor always desirable for this type of structural analysis, but should be checked. The final condition of positivity demands that the mass matrix must be nonnegative, which for structures implies positive definite.

It is assumed that the entire mass of each floor is concentrated at the beam-column joints, with the beam-columns mass being evenly distributed over the six points along the beam column. The masses for the translational degrees of freedom are lumped at the nodes, defined by:

$$m = \frac{1}{2}\int_0^1 m^t_{(x)}dx \qquad \text{..... (16)}$$

The mass is uniform across the beam length, so Equation (16) is simplified to:

$$m = \frac{\bar{m}L}{2} \qquad \text{..... (17)}$$

To be numerically stable, the mass matrix is preferably rank-sufficient and because of the positivity requirement, positive definite. As such, the rotational degrees of freedom are also assigned a rotational inertia. This form of consistent diagonal mass matrix for a uniform member with six degrees of freedom is defined:

$$[\mathrm{M}] = \begin{bmatrix} \frac{\bar{m}L}{2} & 0 & 0 & 0 & 0 & 0 \\ 0 & \frac{\bar{m}L}{2} & 0 & 0 & 0 & 0 \\ 0 & 0 & 3\bar{m}\frac{2}{78} & 0 & 0 & 0 \\ 0 & 0 & 0 & \frac{\bar{m}L}{2} & 0 & 0 \\ 0 & 0 & 0 & 0 & \frac{\bar{m}L}{2} & 0 \\ 0 & 0 & 0 & 0 & 0 & 3\bar{m}\frac{2}{78} \end{bmatrix} \qquad \text{..... (18)}$$

Rayleigh Damping Model

Damping plays an obviously important role in the dynamic analysis of structures. The most effective method of calculating the damping present in a modal analysis form is to treat it as being partly proportional to the relative velocities of the differing degrees of freedom. The equivalent Rayleigh damping is in the form:

$$[C] = \alpha[M] + \beta[K] \qquad \text{..... (19)}$$

Where [*C*] is the assembled damping matrix of the full physical structural system, [*M*] is the assembled mass matrix of the system, [*K*] is the assembled stiffness matrix of the system, and α and β are predefined constants.

Equations of Motion

The incremental equation of motion for the assembled non-linear system can be written:

$$[M]\{\Delta\ddot{u}\} + [C]\{\Delta\dot{u}\} + ([K_L] + [K_G])\{\Delta u\} = \{\Delta F\} \qquad \text{..... (20)}$$

Where [*M*] and [*C*] are the mass and damping matrices respectively, [K_L] and [K_G] are the linear and geometric stiffness matrices, {*F*} is the incremental applied force vector and $\Delta\{\ddot{u}\}, \Delta\{\dot{u}\}$ and $\Delta\{u\}$ are the incremental acceleration, velocity and displacement respectively [7, 8].

Bilinear Strain Hardening Model

Civil structures undergoing large deflections behave non-linearly. To model this behavior a bilinear elas to-plastic hysteresis model is employed. To reflect the non-linear behavior of the response, two linear force-deflection relationships are used with different stiffness values, as shown in Figure (6). This basic behavior will model the strain-hardening property of the material [7].

This model does not take into account a characteristic feature of

Tikrit Journal of Eng. Sciences /Vol.17/No.3/September2010,(22-30)

reinforced concrete. Specifically it does not account for the degradation of unloading and reloading stiffness values. Such degradations are assumed to be small and are ignored in this case. The stress-strain relationship can be expressed as:

$$\varepsilon = \frac{\sigma}{E} \quad \text{for } \sigma \le \sigma_y \qquad \ldots\ldots\ldots\ldots (21)$$

$$\varepsilon = \frac{\sigma_y}{E} + \frac{1}{E_{s1}}(\sigma - \sigma_y) \quad \text{for } \sigma > \sigma_y \ \ldots (22)$$

Modeling of Blast Loading

Relatively distant blast loads are typically characterized by a rapid rise in pressure followed by decay back to atmospheric pressure. Some amount of reverse pressure usually occurs following the decay period, but this level is usually small and ignored here [4]. In this study, the blast load is modeled as a simple triangular wave that acts over a small period and displays no reverse pressure as shown in Figure (7) **[4]**. It is modeled using equivalent point loads, based on pressure and applied area, at each story. During a blast, structures are subjected either to ground shaking (in cases of underground explosion) or to lateral pressure (common for air-blast). In either case, the ground shaking or the lateral pressure is of an impulsive nature, with a high peak and short duration. In this study, the blast load is modeled as a point load, *P*, acting on the top of the left column of the structure, as shown in Figure (8). The point load, *P*, is in Newtons, which is obtained by multiplying the blast-induced pressure by the area it acts upon, which is assumed to be half the force area.

Numerical Model

To understand how a tendon located at different points on a structure responds to a blast load, three-story structure is modeled in this study. From the prospective parametric analysis of these simple multi-story structures, a general tendon layout and design approach can be determined to best resist the effects of blast loads in a general sense.

The frame used in the analyses in this study is assumed to be reinforced concrete. As shown in Figure (9), the frame is 3.6 meters wide and 10.8 meters tall. The structure is designed so that it has a natural frequency of 0.7Hz. The beam and column frame members have the same 300mm x 300mm cross-section with an elastic modulus of 10 GPa. The structure is modeled using nonlinear finite elements employing a bilinear hysteretic model that degrades to 5% of the pre-yield stiffness during yielding as shown in Figure (10). The frame is analyzed using a non-linear, elastic-plastic finite element program written in MATLAB.

Six tendon architectures were investigated as shown in Figure (11). A single tendon was placed between different floors and its effects investigated. The ideal case will be that which reduces the maximum displacement, the amount of permanent deflection and not increase the maximum structural shear forces greatly. In other words, a tendon that will reduce displacement but keep shear at a safe level for foundation capacity is the desired solution. The blast wave is modeled as a simple triangle wave with a peak of 35kN and a width of 0.05 seconds.

Results

The maximum displacement response of the structure with and without the tendon is plotted against the structural period in Figure (12). As the structural period increases, the magnitude of the first displacement peak decreases. Above a period of 1 or 2 seconds the reduction

in peak displacement remains effectively constant for all structural periods.

The permanent deflection, shown in Figure (13), shows a trend similar to the peak displacement. For periods above arranged in the form of six cases as in Figure (11) and exposed to a 35kN blast load. The tendon arrangements going from the ground to the second and third floors (arrangements 2 and 3) reduce the size of the first peak displacement, as shown in Figure (14). The ground to second floor arrangement is the slightly more effective of the two architectures as shown in Figure (15). Arrangements with the tendon attached between the story, rather than to the ground, do not perform well. However, as shown in Figure (15), these arrangements may lead to further reduce in the amount of permanent deflection in some cases.

Figure (16) shows the induced base shear. The arrangements that do not involve the ground have the least effect on the base shear, as expected. The ground to second floor increases the base shear by the smallest margin when compared to the other arrangements involving the ground.

Conclusions

1. The effectiveness of the tendon is greatest for structures with lower periods, where higher modes are less excited. Thus, for structural periods greater than 1 or 2 seconds a tendon may not be warranted.
2. The results indicate that a tendon spanning from the ground to approximately two thirds the height of the structure would perform the best, reducing the displacement by the greatest amount with a smaller cost in increased base shear, as compared to the other effective tendon arrangements.

1 second the reduction in the permanent deflection is minimal with the tendon.

Figures (14-16) show the effect of using a 30kN tendon (fails at 30kN)

References

1. Stewart M. G, Netherton MD, Rosowsky DV, "Terrorism Risks and Blast Damage to Build Infrastructure", Natural Hazards Review ASCE, pp. 1527-6988 (2006).
2. Dhakal RP, Pan T-C. "Response Characteristics of Structures Subjected to Blasting Induced Ground Motion". International Journal of Impact Engineering 28, pp. 813-828 (2003).
3. Gantes CJ, Pnevmatikos NG., "Elastic-plastic Response Spectra for Exponential Blast Loading", International Journal of Impact Engineering 30, pp. 323-343 (2004).
4. Mays, G C and Smith, P D (Ed), "Blast Effects on Buildings Design of Buildings to Optimize Resistance to Blast Loading," Thomas Telford, pp. 210-318(1995)
5. Lu Yong, Hao Hong, Ma Guowei, Zhou Yingxin. "Simulation of Structural Response under High Frequency Ground Excitation". Earthquake Engineering and Structural Dynamics 30, pp. 307-325 (2001).
6. Giberson, Melborne F., "Two Nonlinear Beams with Definitions of Ductility," Journal of the Structural Division, ASCE, Vol. 95, No. ST2, Proc. Paper 6377, pp. 137-157, February (1969).
7. Dong, Ping, “Effect of Varying hysteresis Models and Damage Models on Damage Assessment of r/c Structures Under Standard Design Level Earthquakes Obtained

Tikrit Journal of Eng. Sciences /Vol.17/No.3/September2010,(22-30)

Using a New Scaling Method," PhD thesis, Department of Civil Engineering, University of Canterbury, Christchurch, New Zealand, pp. 123-202, (2003).

8. Bathe, Klaus-Jürgen, "Finite element procedures in engineering analysis," Prentice- Hall, New Jersey, pp. 117-128, (1982).

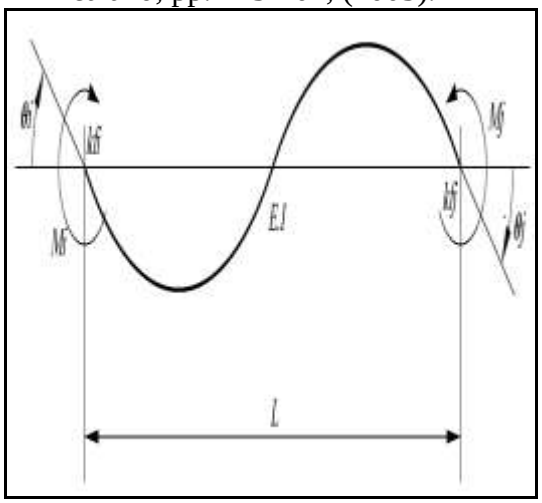

Figure (1): Giberson one-component Model

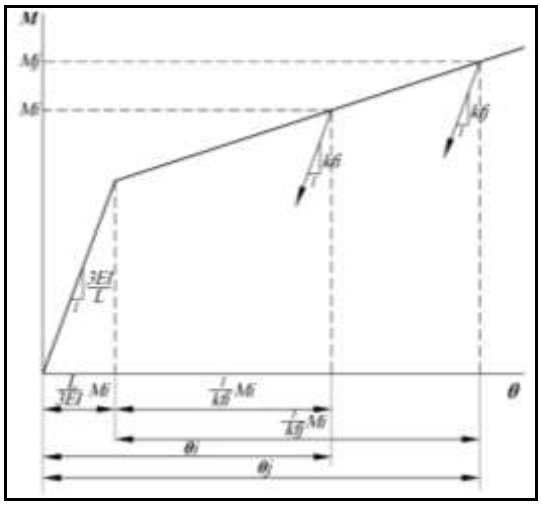

Figure (2): Moment-Rotation Relations at the Member End

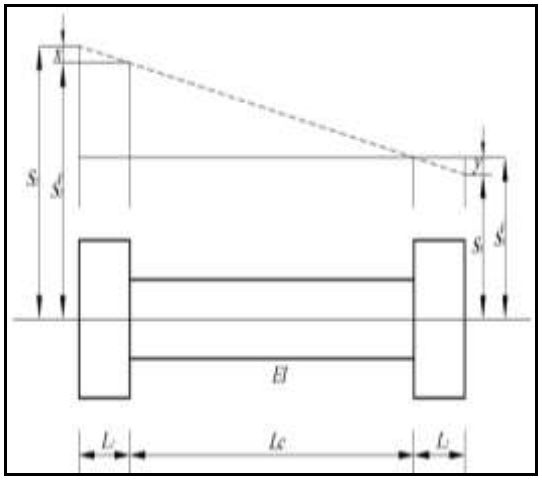

Figure (3): Model for Member with Rigid End-block

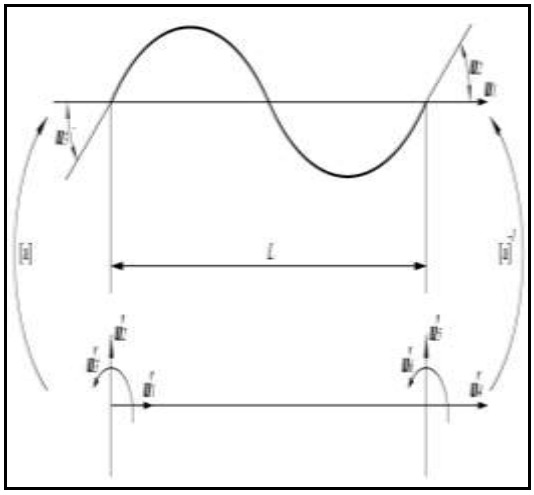

Figure (4): the 3 Relative Displacements (Upper) and the 6 Nodal Displacements (Lower) in the Local Coordinate System

Tikrit Journal of Eng. Sciences /Vol.17/No.3/September2010,(22-30)

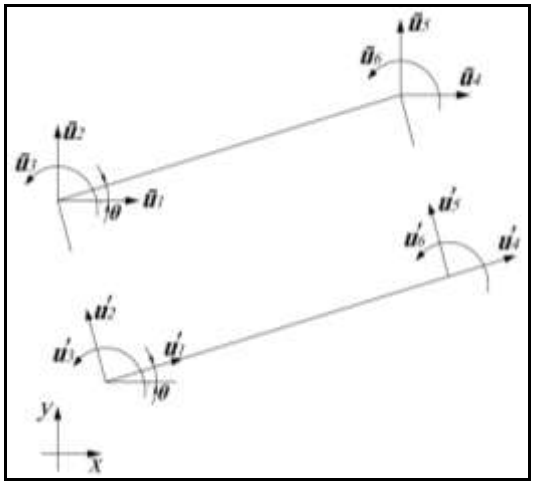

Figure (5): Local and Global Coordinate Systems

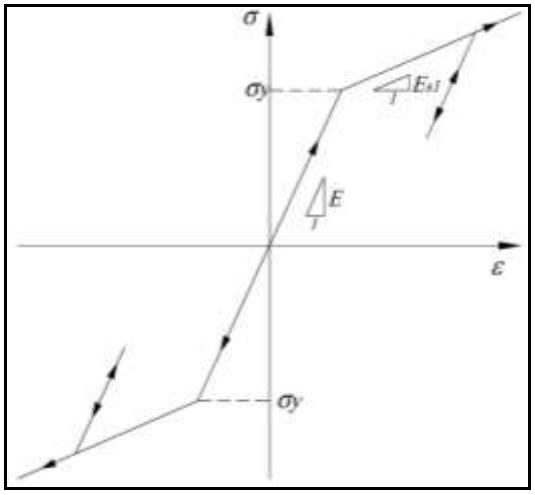

Figure (6): Bilinear Hysteresis Model

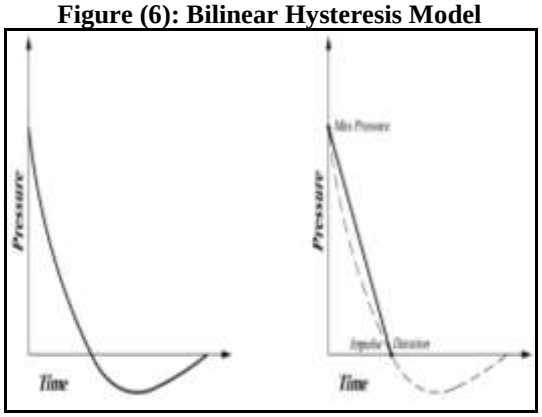

Real Pressure History Simplified Pressure History

Figure (7): Modelled Blast Load

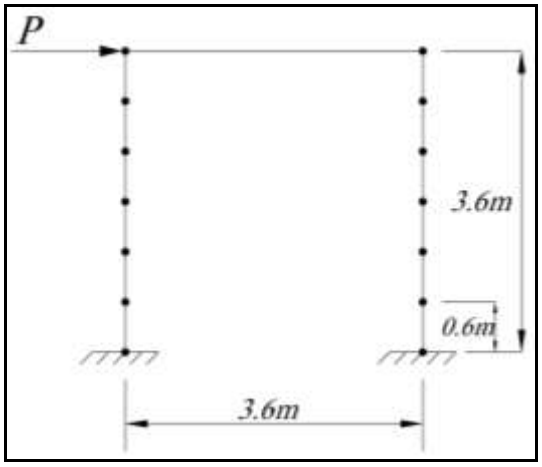

Figure (8): One-Story Layout

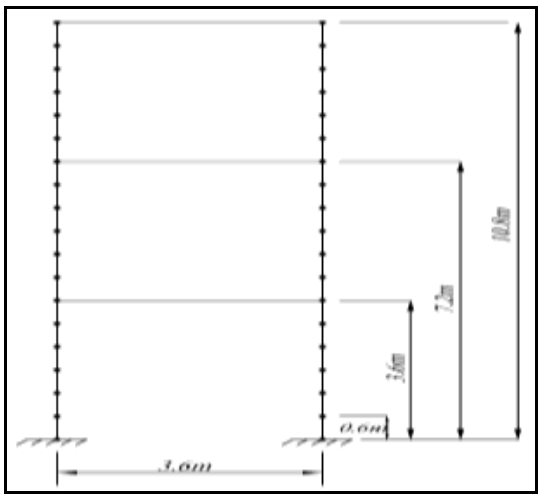

Figure (9): General Model Configuration

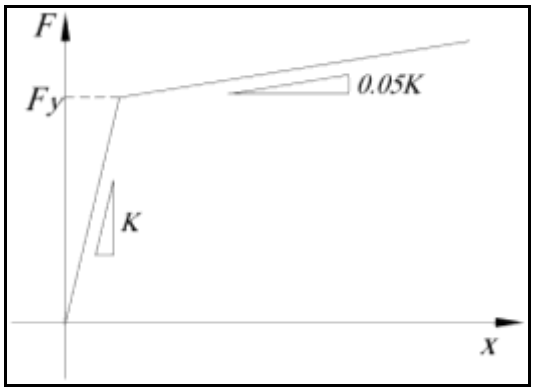

Figure (10): Bilinear Hysteretic Model

Tikrit Journal of Eng. Sciences /Vol.17/No.3/September2010,(22-30)

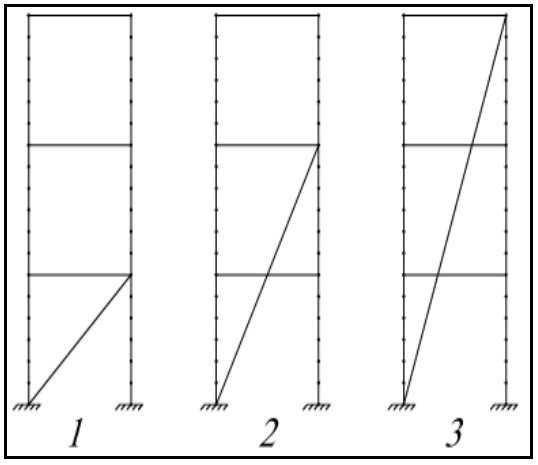

Figure (11): Tendon architectures

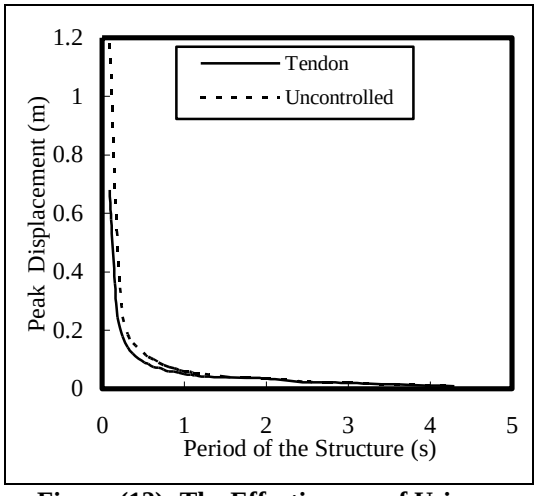

Figure (12): The Effectiveness of Using a Tendon on Peak Displacement

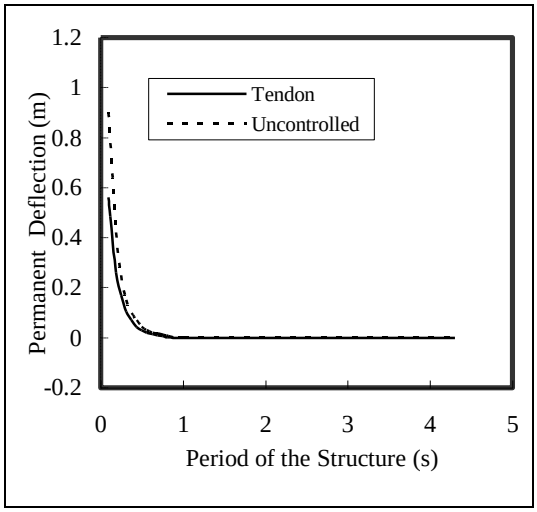

Figure (13): The Effectiveness of Using a Tendon on Permanent Deflection

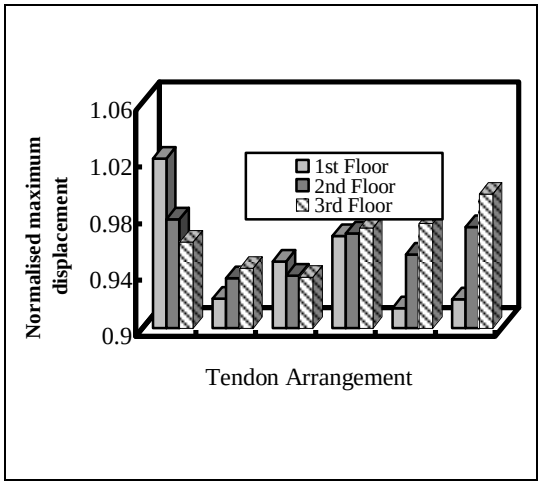

Figure (14): Structural Responses (Peak Displacement)

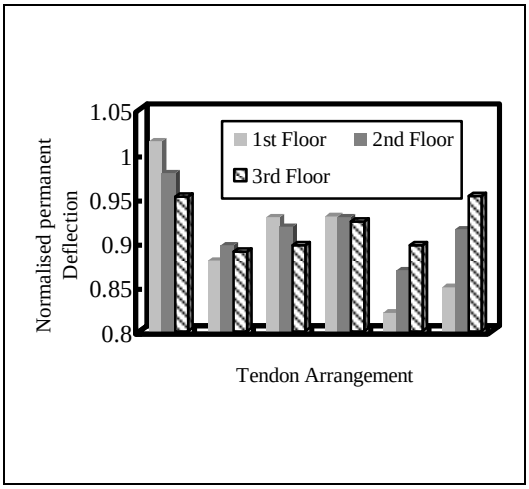

Figure (15): Structural Responses (Permanent Deflection)

Tikrit Journal of Eng. Sciences /Vol.17/No.3/September2010,(22-30)

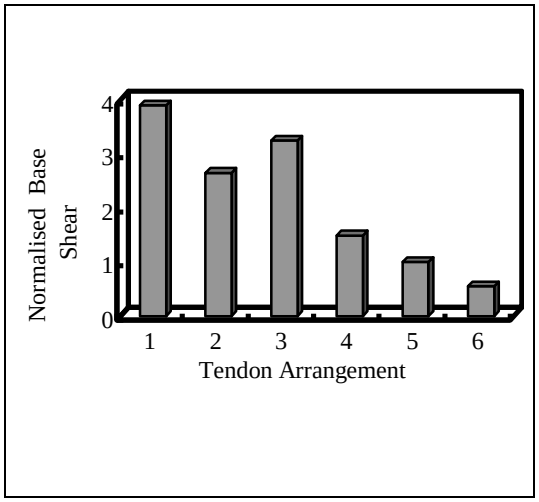

Figure (16): Structural Responses (Normalized Base Shear)